

Phase-sensitive manipulation of squeezed state by a degenerate optical parametric amplifier inside coupled optical resonators*

DI Ke, WANG Wenbo, CUI Wei, GUO Junqi, LIU Yu, and DU Jiajia**

Chongqing Engineering Research Center of Intelligent Sensing Technology and Microsystem, Chongqing University of Post and Telecommunications, Chongqing 400065, China

(Received 16 September 2021; Revised 24 September 2021)

©Tianjin University of Technology 2022

In this paper, we investigate the quantum fluctuations of subharmonic reflected field from a triple-resonant degenerate optical parametric amplifier (OPA) inside coupled optical resonators, which is driven by the squeezed beam at signal frequency. By controlling the relative phase between the pump beam and the injected signal beam, we can see the quantum fluctuation in the phase direction and amplitude direction due to the parametric down-conversion process in the cavity. Thus, the phase sensitive operation of the compression field is realized due to the quantum interference between the harmonic field of the down converter of OPA and the inner field of the coupled optical resonator. We verified the quantum coherent phenomena of OPA in coupled optical resonators and phase-sensitive manipulations of quantum entanglement for quantum information processing. We realized the electromagnetically induced transparency-like (EIT-like) effect and the optical parameter conversion process at the same time in one optical device. These properties can favor higher manipulation precision and control efficiency, which is more suitable for the integration of quantum-on-chip systems, laying a foundation for the practical application of quantum information.

Document code: A **Article ID:** 1673-1905(2022)03-0135-8

DOI <https://doi.org/10.1007/s11801-022-1149-z>

The optical parametric amplification process is an important nonlinear phenomenon, which has a wide range of applications in the fields of quantum optics, such as laser generation, frequency conversion, etc^[1]. It can generate and manipulate light fields in non-classical states, and optical parametric amplification (OPA) technology has been proven to be an effective method to generate light fields in continuous compressed state^[2,3]. In the past few decades, people have done a lot of work, hoping that the compressed state can be applied to weak signal detection, accurate measurement and quantum information processing, such as entangled state preparation, optical phase estimation, gravity wave measurement and sample transmittance measurement^[4-6]. Recently, ZHANG et al^[7] have verified a quantum guided ellipsoid in an experiment and tested its volume uniformity. The volume of the ellipsoid does not depend on the reference system. This work not only deepens people's understanding of the non-locality of quantum guidance, but also lays an important foundation for the quantum guidance ellipsoid as a reference

frame-independent quantum correlation diagnostic tool.

Electromagnetic induced transparency (EIT) is a physical phenomenon caused by quantum interference between atomic states caused by the interaction of coherent electromagnetic field and multi-level atomic system, which makes the opaque medium transparent to the detection light^[8,9]. The EIT-like effect is mainly the EIT effect in the classical field. In this paper, the EIT transmission spectrum similar to that in the atomic system can be obtained by externally adjusting the detuning amount of the resonant wavelength of two cavities and the phase difference detuning amount between the two cavities through the coupling of several micro-cavities.

In this paper, the quantum fluctuation and coherence of OPA cavity of type I nonlinear crystal coupled with beam under vacuum compression are theoretically discussed. These phenomena are caused by the interference between the harmonic field and the subharmonic field in the resonator^[10]. We selected the appropriate length of the degenerate optical parametric amplifier (DOPA) cavity and the

* This work has been supported by the National Natural Science Foundation of China (Nos.11704053, 61705027 and 62005033), the National Key R&D Program of China (Nos.2018YFF01010202 and 2018YFF01010201), the Science and Technology Research Program of Chongqing Municipal Education Commission (Nos.KJQN201800629 and KJQN201800621), the Innovation Leader Talent Project of Chongqing Science and Technology (No.CSTC-CXLJRC201711), the Postdoctoral Applied Research Program of Qingdao (No.62350079311135), and the Postdoctoral Applied Innovation Program of Shandong (No.62350070311227).

** E-mail: dujj@cqupt.edu.cn

reflection coefficients of the front and rear mirrors, then injected the signal beam and pump beam from both ends of the OPA cavity^[11-13]. By observing the down-conversion of the harmonic field under the intermediate cavity mirrors with different reflection coefficients, the line shape caused by the quantum interference between the lower stages and the line generated under different interferences will also show different structures^[14]. In addition, the appropriate relative phase between the pump beam and signal beam can increase the degree of interference. Since the model can simultaneously manipulate the EIT-like effect and the optical parameter conversion process, the integration and operability of the on-chip system are greatly improved in the chip manufacturing^[15,16].

We consider a simple Fabry-Perot (F-P) cavity, which consists of two common cavity mirrors (M_{fron} and M_{bac}), and then the plane cavity mirror (M_{mid}) is placed in the center of the F-P cavity to form the coupled optical resonators. Finally, a periodically poled KTiOPO₄ (PPKTP) crystal is placed in the right optical cavity to complete the whole installation^[16]. As shown in Fig.1, the light fields with frequencies of ν and 2ν respectively represent the sub-harmonic field and the harmonic field. Assuming that the resonator is a standing wave cavity with length of L (round trip time is $\tau=2L/c$), the reflectivities of M_{fron} and M_{mid} to the sub-harmonic field are r_{1a} and r_{2a} , respectively. The reflectivities of the harmonic field are r_{2b} and r_{1b} . The reflectivity of the M_{bac} mirror relative to the harmonic field is R_b , which has high reflectivity for sub-harmonic fields. When the vacuum squeezed beam is injected from the M_{fron} cavity mirror and the pump beam is injected from the M_{bac} cavity mirror, we can observe the shape of the spectrum under different interference conditions by understanding the reflectivity of the M_{mid} cavity mirror^[17,18].

It is obvious that the reflection coefficient of the left cavity can be calculated respectively as

$$R_{\text{in}}^a = \frac{r_{2a} - r_{1a}^* a_1^* e^{i\varphi_1}}{1 - r_{1a}^* r_{2a}^* e^{i\varphi_1}}, \quad (1)$$

$$R_{\text{in}}^b = \frac{r_{2b} - r_{1b}^* a_2^* e^{i\varphi_2}}{1 - r_{1b}^* r_{2b}^* e^{i\varphi_2}}, \quad (2)$$

where $\varphi_j = \frac{2\pi 2L_j n_j \omega}{c}$ is the phase variation during a round trip in the cavity, which has the signal beam frequency ω with the length of the cavity L_j and the refractive index n_j . a_i is the loss caused by a round trip in the cavity, and j is the corresponding optical cavity^[19].

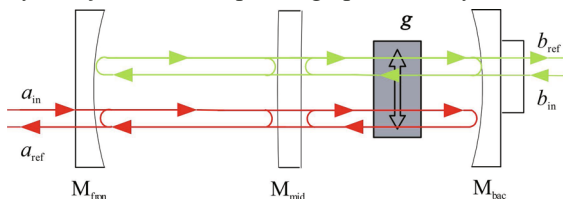


Fig.1 Schematic of a triple-resonant optical parametric amplifier inside a standing-wave cavity

The equations of motion for the subharmonic and harmonic fields are described by the semiclassical method as

$$\tau \frac{da}{dt} = -i\Delta_a \tau a - \gamma_a a + g b a^* + \sqrt{2\gamma_{\text{ina}}^c} a_{\text{in}} + \sqrt{2\rho^a} a_v, \quad (3)$$

$$\tau \frac{db}{dt} = -i\Delta_b \tau b - \gamma_b b + \sqrt{2\gamma_{\text{in}}^b} b_{\text{in}} + \sqrt{2\rho^b} b_v, \quad (4)$$

where a_v and b_v are coupled into the subharmonic and harmonic fields and γ_a is the total damping of the subharmonic field expressed as $\gamma_a = \gamma_{\text{ina}}^c + \rho^a$, where ρ^a is the decay rate for internal losses, $\gamma_{\text{ina}}^c = (1 - R_{\text{in}}^a)/2$ is the damping associated with coupling mirror M_{fron} and M_{mid} , γ_b is the total damping of the harmonic field expressed by $\gamma_b = \gamma_{\text{in}}^b + \rho^b$, where $\rho^b = \gamma_{\text{inb}}^c + \rho$ is the decay rate for internal losses and similarly $\gamma_{\text{in}}^b = (1 - R_b)/2$ is the damping associated with coupling mirror M_{bac} ^[20-22].

From Eq.(4), we can work out the change of pump beam running trip in the cavity, while the first term on the right is the losing harmonic term, the second term is the loss term and the last term is the input term. Since the pump beam is steady state, the left-hand side of Eq.(4) is 0, and we can obtain

$$\tau \frac{da}{dt} = -i\Delta_a \tau a - \gamma_a a + g \frac{\sqrt{2\gamma_{\text{in}}^b} |b_{\text{in}}| a^* e^{i\theta}}{\gamma_b + 2i\Delta\tau} + \sqrt{2\gamma_{\text{ina}}^c} a_{\text{in}} + \sqrt{2\rho^a} a_v. \quad (5)$$

Fourier transform and linearization of Eq.(6) can be obtained by noise from the amplitude and phase directions as

$$\begin{aligned} \langle \delta^2 X_o^a(\omega) \rangle = & \{ \{ [2\sqrt{2\gamma_{\text{in}}^b} g \gamma_{\text{ina}}^c |b_{\text{in}}| (\gamma_b \cos \theta + 2\Delta\tau \sin \theta) + 2\gamma_{\text{ina}}^c (\gamma_b^2 + 4\Delta^2 \tau^2) \gamma_a + 2g^2 \gamma_{\text{in}}^b |b_{\text{in}}|^2 - (\gamma_b^2 + 4\Delta^2 \tau^2) [\gamma_a^2 + (\Delta^2 - \omega^2) \tau^2] \}^2 + \\ & [2(\gamma_b^2 + 4\Delta^2 \tau^2) \omega \tau (\gamma_{\text{ina}}^c - \gamma_a)] \} \langle \delta^2 X_{\text{in}}^a(\omega) \rangle + \\ & [2\gamma_{\text{ina}}^c (\gamma_b^2 + 4\Delta^2 \tau^2) \Delta\tau + 2\sqrt{2\gamma_{\text{in}}^b} g \gamma_{\text{ina}}^c |b_{\text{in}}| \times (\gamma_b \sin \theta - 2\Delta\tau \cos \theta)]^2 \langle \delta^2 Y_{\text{in}}^a(\omega) \rangle + \\ & \{ [2g\sqrt{2\gamma_{\text{in}}^b} \gamma_{\text{ina}}^c \rho^a |b_{\text{in}}| (\gamma_b \cos \theta + 2\Delta\tau \sin \theta) + 2\sqrt{\gamma_{\text{ina}}^c \rho^a} (\gamma_b^2 + 4\Delta^2 \tau^2) \gamma_a]^2 + \\ & [2\sqrt{\gamma_{\text{ina}}^c \rho^a} (\gamma_b^2 + 4\Delta^2 \tau^2) \omega \tau]^2 \} \langle \delta^2 X_v^a(\omega) \rangle + \\ & [2\sqrt{\gamma_{\text{ina}}^c \rho^a} (\gamma_b^2 + 4\Delta^2 \tau^2) \Delta\tau + 2g\sqrt{2\gamma_{\text{in}}^b} \gamma_{\text{ina}}^c \rho^a |b_{\text{in}}| (\gamma_b \sin \theta - 2\Delta\tau \cos \theta)]^2 \times \\ & \langle \delta^2 Y_v^a(\omega) \rangle \} / \{ [(\gamma_b^2 + 4\Delta^2 \tau^2) [\gamma_a^2 + (\Delta^2 - \omega^2) \tau^2] - 2g^2 \gamma_{\text{in}}^b |b_{\text{in}}|^2 + [2(\gamma_b^2 + 4\Delta^2 \tau^2) \omega \tau \gamma_a]^2 \}, \\ \langle \delta^2 Y_o^a(\omega) \rangle = & \{ \{ [-2\sqrt{2\gamma_{\text{in}}^b} g \gamma_{\text{ina}}^c |b_{\text{in}}| (\gamma_b \cos \theta + \end{aligned}$$

$$\begin{aligned}
& 2\Delta\tau \sin\theta) + 2\gamma_{\text{ina}}^c (\gamma_b^2 + 4\Delta^2\tau^2)\gamma_a + 2g^2\gamma_{\text{in}}^b |b_{\text{in}}|^2 - \\
& (\gamma_b^2 + 4\Delta^2\tau^2)[\gamma_a^2 + (\Delta^2 - \omega^2)\tau^2]^2 + \\
& [2(\gamma_b^2 + 4\Delta^2\tau^2)\omega\tau(\gamma_{\text{ina}}^c - \gamma_a)]^2 \langle \delta^2 Y_{\text{in}}^a(\omega) \rangle + \\
& [-2\gamma_{\text{ina}}^c (\gamma_b^2 + 4\Delta^2\tau^2)\Delta\tau + 2\sqrt{2\gamma_{\text{in}}^b} g\gamma_{\text{ina}}^c \times \\
& |b_{\text{in}}| (\gamma_b \sin\theta - 2\Delta\tau \cos\theta)]^2 \langle \delta^2 X_{\text{in}}^a(\omega) \rangle + \\
& \{[-2g\sqrt{2\gamma_{\text{in}}^b}\gamma_{\text{ina}}^c\rho^a |b_{\text{in}}| (\gamma_b \cos\theta + 2\Delta\tau \sin\theta) + \\
& 2\sqrt{\gamma_{\text{ina}}^c\rho^a} (\gamma_b^2 + 4\Delta^2\tau^2)\gamma_a]^2 + \\
& [2\sqrt{\gamma_{\text{ina}}^c\rho^a} (\gamma_b^2 + 4\Delta^2\tau^2)\omega\tau]^2 \langle \delta^2 Y_v^a(\omega) \rangle + \\
& [-2\sqrt{\gamma_{\text{ina}}^c\rho^a} (\gamma_b^2 + 4\Delta^2\tau^2)\Delta\tau + \\
& 2g\sqrt{2\gamma_{\text{in}}^b}\gamma_{\text{ina}}^c\rho^a |b_{\text{in}}| (\gamma_b \sin\theta - 2\Delta\tau \cos\theta)]^2 \times \\
& \langle \delta^2 X_v^a(\omega) \rangle\} / \{[(\gamma_b^2 + 4\Delta^2\tau^2)[\gamma_a^2 + \\
& (\Delta^2 - \omega^2)\tau^2] - 2g^2\gamma_{\text{in}}^b |b_{\text{in}}|^2]^2 + \\
& [2(\gamma_b^2 + 4\Delta^2\tau^2)\omega\tau\gamma_a]^2\}, \quad (6)
\end{aligned}$$

where $\langle \delta^2 X_{\text{in}}^a(\omega) \rangle = e^{-2s}$ and $\langle \delta^2 Y_{\text{in}}^a(\omega) \rangle = e^{2s}$ represent the noise fluctuations in the amplitude and phase directions of the input field individually, and s is the compression exponent. Here, $\langle \delta^2 X_{\text{in}}^a(\omega) \rangle = 1$, $\langle \delta^2 Y_{\text{in}}^a(\omega) \rangle = 1$ because it is the vacuum input field.

The coupling strength of the coupled resonator depends on the transmittance of the M_{mid} cavity mirror. According to the reflection coefficient of the intermediate cavity mirror of the signal field and the pump field, we will study the quantum fluctuations in the two cases of weak quantum interference and strong quantum interference in the coupled cavity within a period.

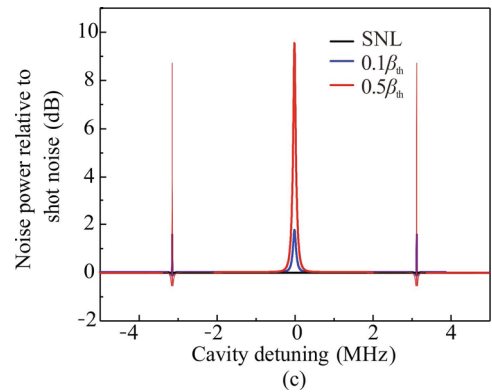
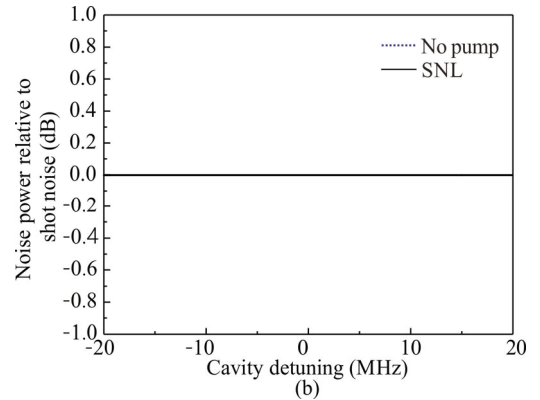
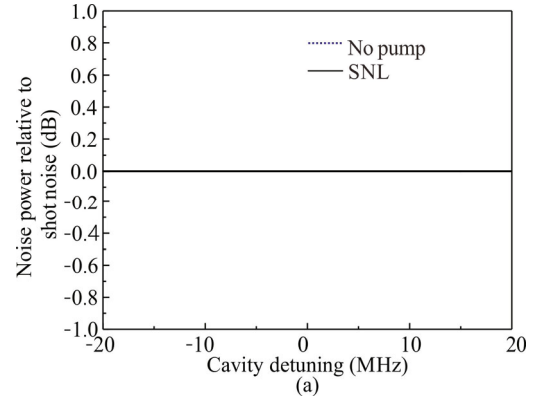
Case 1 The intermediate cavity mirror loss in the signal field is set as $r_{1a}=0.00016$, when the M_{mid} cavity mirror loss in the pumping field is set as $r_{2b}=0.002$. The specific cavity parameters are shown in Tab.1. In this instance, both the signal field and the pump field are weakly interfered.

Tab.1 Loss coefficient of each cavity mirror under weak interference of signal field and pump field

Parameter	Loss
r_{1a}	0.00016
r_{2a}	0.00016
r_{1b}	0.01
r_{2b}	0.002
ρ^a	0.0005
ρ^b	0.01
γ_{in}^b	0.0001

Case 1 (a) We study the vacuum beam field as a signal field. As shown in Fig.2(a) and Fig.2(b), when there is no pump beam injected, there is no noise fluctuation in the amplitude and phase directions due to parameter

conversion in the cavity. The pump beam is now injected, and when the phase difference between the vibration and the signal beam is $\Phi=0$, the noise fluctuation curve in the amplitude direction of the OPA reflective chamber is shown in Fig.2(c). The blue curve is a noise curve when the pump beam intensity is $0.1\beta_{\text{th}}$. It can be seen that the noise curve is enlarged due to quantum interference at zero detuning. Inverted Lorentz curves with splits due to EIT-like phenomena appear at the far detuning. At the same time, as the pump beam intensity increases to $0.5\beta_{\text{th}}$, the near and far detuning gains are further amplified. When $\Phi=\pi/2$, the noise curve in the phase direction is shown in Fig.2(d). When the detuning is zero, the noise curve drops below the shot noise limit (SNL). Similarly, the EIT-like effect appears at the far detuning. When the pump beam increases to $0.5\beta_{\text{th}}$, the compression at zero detuning is further amplified, and the gain at far detuning also increases as the intensity of the pump beam increases.



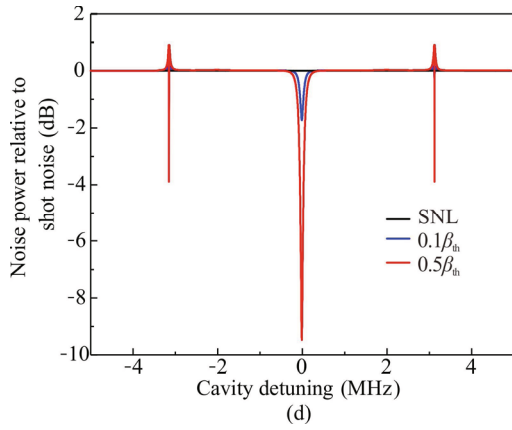


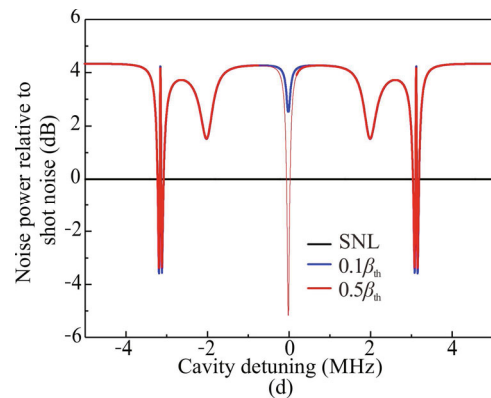
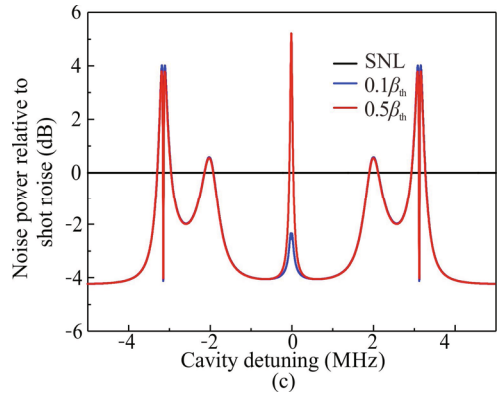
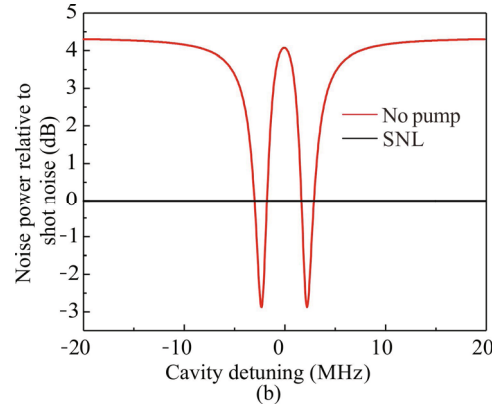
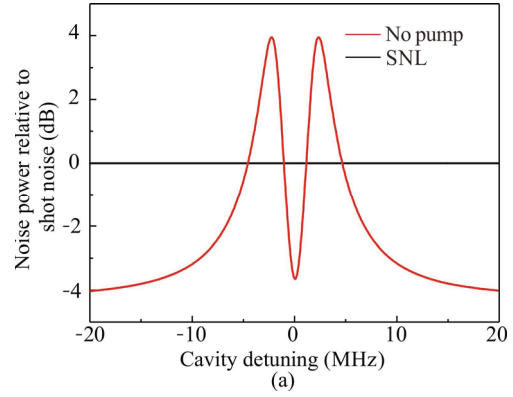
Fig.2 Quantum correlation noise fluctuation curves in the vacuum field of the weakly coupled resonant cavity under three resonance cases: Noise curves in the (a) amplitude and (b) phase directions without pump light injection; Noise curves in the (c) amplitude and (d) phase directions when $\theta=0$ (The black curves are the shot noise limit (SNL), the blue curves are for the pump light intensity of $0.1\beta_{th}$, and the red curves are for the pump light intensity of $0.5\beta_{th}$)

Case 1 (b) Now the case of injected vacuum squeezed beam field as the signal field is studied, and the noise fluctuation curve of the reflected field is shown in Fig.3.

The M_{bac} cavity is closed, leaving only the front cavity. Then the compressed beam, as signal beam, is injected into the cavity, and the noise fluctuation curve of the OPA reflected light field is shown in Fig.3(a) and Fig.3(b). When the phase difference between the local oscillation beam and the signal beam is $\Phi=0$, the amplitude noise curve is at zero detuning because the maximum transmission causes the compression intensity to be lower than that of the incident light field. While at the near detuning, the compression becomes inverse compression due to the influence of quantum interference. When $\Phi=\pi/2$, the noise fluctuation curve in the phase direction and the amplitude direction are symmetrical.

Now the M_{bac} cavity mirror is turned on and the pump beam is injected. At the pumping intensity of $0.1\beta_{th}$, as shown in Fig.3(c), the compression intensity decreases at the resonance due to the maximum transmission of the quantum OPA cavity, and a depression appears at the center of the noise curve. At the far resonance, a Lorentz curve with cleavage appears due to the EIT-like effect of the coupled cavity and a small peak appears at the valley. When the pump light intensity increases to $0.5\beta_{th}$, the noise profile at zero detuning changes from compression to amplification, and the height of the small peak increases at far detuning with the increase of the pump light intensity. When the phase difference between the local oscillation beam and the signal beam is $\Phi=\pi/2$, the noise curve in the phase direction is shown in Fig.3(d).

When the pump beam intensity is $0.1\beta_{th}$, the noise curve is lost due to the noise of the resonance when the detuning is zero, and the EIT-like effect at the far detuning appears here as an inverted Lorentz curve with split.



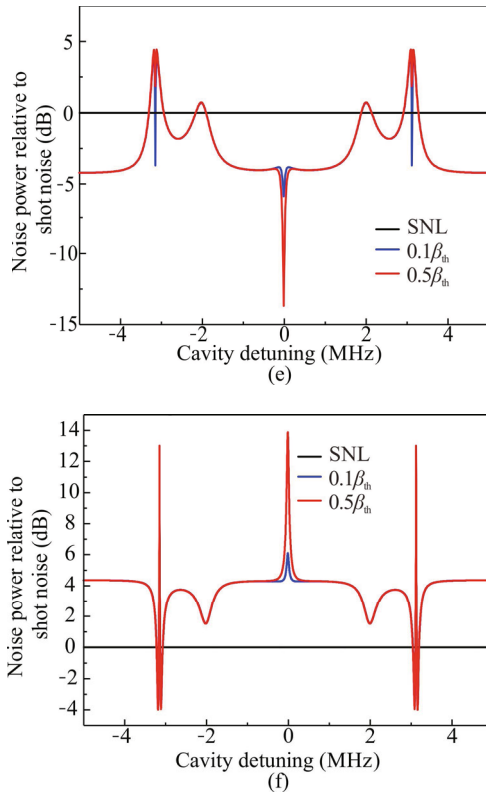


Fig.3 Quantum correlation noise fluctuation curves in the vacuum compression field of the weakly coupled resonant cavity under three resonance cases: Noise curves in the (a) amplitude and (b) phase directions without pump light injection; Noise curves in the (c) amplitude and (d) phase directions when $\theta=0$; Noise curves in the (e) amplitude and (f) phase directions when $\theta=\pi$

Fig.3(e) and Fig.3(f) show the noise distributions when the phase difference between the signal and pump beams is $\theta=\pi$. At zero detuning, the compression in the amplitude direction changes from reverse amplification at $\theta=0$ to further compression and is positively correlated with the intensity of the pump beam. Because of the EIT-like effect, the noise fluctuation curve at the far detuning appears as a Lorentz curve with split. The noise fluctuation curves in the phase direction show a spike at zero detuning due to quantum interference. At the far detuning, the inverted Lorentz curve shape with splits also appears due to the EIT-like effect.

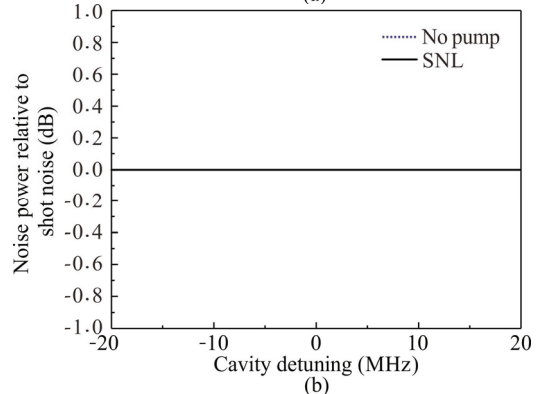
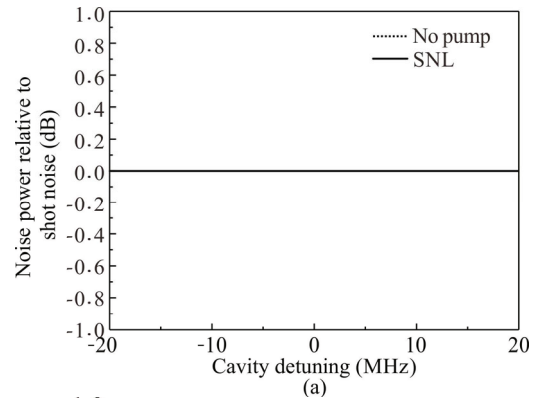
Case 2 Now the quantum fluctuation reflected from strongly interfered system injected with the squeezed vacuum beam is studied, when $r_{1a}=0.16$, $r_{2b}=0.02$, and the other parameters are constant. The specific cavity parameters are shown in Tab.2.

Case 2 (a) When the vacuum beam field is used as the signal beam field, as shown in Fig.4(a) and Fig.4(b), since there is no pumping beam input, no parameter conversion occurs in the cavity, so the noise curves in the amplitude and phase directions are the same as those of the SNL.

Tab.2 Loss coefficient of each cavity mirror under strong interference of signal field and pump field

Parameter	Loss
r_{1a}	0.16
r_{2a}	0.016
r_{1b}	0.01
r_{2b}	0.002
ρ^a	0.000 5
ρ^b	0.01
γ_{in}^b	0.000 1

Now pump beam is injected. When the phase difference between the local beam and signal beam as $\Phi=0$, the noise amplitude direction curve as shown in Fig.4(c). When the detuning is zero, the influence of the quantum interference makes noise curve be amplified to higher than SNL curve. In far detuning an inverted Lorentz curve with a split is formed because of the influence of the type of EIT-like effect in left and right sides. When the pumping beam intensity is increased to $0.5\beta_{th}$, the gain of the noise curve is significantly enhanced. When $\Phi=\pi/2$, the noise curve in the phase direction is dented at the zero detuning, and Lorentz curve with split is formed at the far detuning due to the EIT-like effect. When the pump beam intensity is increased to $0.5\beta_{th}$, the depression at zero detuning is further amplified, and the gain at far detuning is amplified again due to EIT-like effect. Compared with Case 1 (a), the quantum manipulation effect on amplitude and phase directions in the case of strong interference is stronger than that in the case of non-interference, and EIT-like effect is more significant in the case of strong interference.



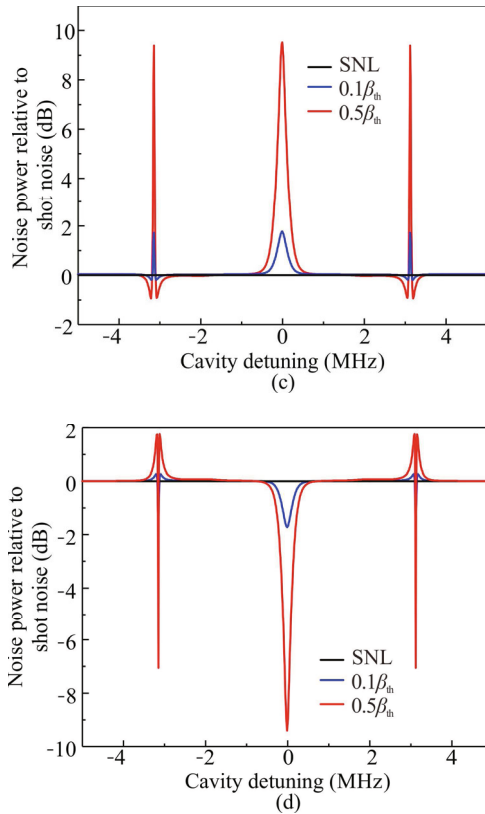


Fig.4 Quantum correlation noise fluctuation curves in the vacuum field of weakly and strongly combined resonant cavities under three resonance cases: Noise curves in the (a) amplitude and (b) phase directions without pump light injection; Noise curves in the (c) amplitude and (d) phase directions when $\theta=0$

Case 2 (b) Now, the situation of injecting a squeezed vacuum is researched, whose noise fluctuations of the reflected field are shown in Fig.5.

When the M_{front} cavity is closed, only the anterior cavity is retained without pump beam injected, as shown in Fig.5(a) and Fig.5(b). At zero detuning, the compression intensity is further compressed relative to the incident beam field due to the effect of quantum interference, and at near detuning, the compression becomes reverse compression due to the effect of quantum interference. As for the noise fluctuation curve in the phase direction, when the detuning is zero, the intensity of the noise curve is the same as that of the incident beam field. However, the noise curve near the detuning turns amplification into compression due to the influence of quantum interference.

Compared with Case 1 (b), the half-width of the noise fluctuation curve in the amplitude and phase directions in the strong interference case is wider than that in the interference case, and the quantum interference has a wider impact.

Now, by turning on the rear cavity mirror to inject the pump beam, we can find efficient quantum manipulation due to a second-order nonlinear optical process. When

relative phase is $\theta=0$, the noise on amplitude of direction curve is shown in Fig.5(c). Due to the resonance at zero detuning, at the same time, here, a little cleavage appears because of the influence of the quantum interference effect. In far detuning, the noise curve shows a depression due to the quantum interference. At the same time, due to the EIT-like effect in the coupling cavity, Lorentz curve with split and small peaks is formed at the left and right ends. When the pump beam intensity is increased to $0.5\beta_{th}$, the noise curve at zero detuning increases directly from the compression state to the amplification state, and the small peak at the far detuning is further amplified directly and presents a three-peak structure.

When $\Phi=\pi/2$, the noise curve in the phase direction appears a depression and a small peak due to the influence of quantum interference. At the far detuning, the amplification turns into compression to form the depression. At the same time, due to the EIT-like effect, the inverted Lorentz curve with split is formed at the far detuning, and the depression appears in the case of strong interference. As the pump intensity is increased to $0.5\beta_{th}$, the amplification at the zero detuning becomes compression, and the depression in the inverted Lorentz curve at the far detuning is further compressed below SNL. When the phase difference between the signal beam and the pump beam as $\theta=\pi$, the noise curve in the amplitude direction is further compressed at zero detuning due to the influence of quantum interference, which is higher than the compression intensity of the field. Similarly, Lorentz curve is formed at far detuning due to the EIT-like effect. When the pump beam is further increased to $0.5\beta_{th}$, the compression at zero detuning is further enhanced. The gain at the far detuning is more significant. The noise curve in the phase direction shows a small peak higher than the incident beam field at zero detuning, and the inverted Lorentz curve with split like EIT-like effect appears on both sides. With the increased intensity of the pumping beam, the amplification is further enhanced. Above analyses show that the quantum manipulation effects of coupled OPA amplifying cavity are different under different interferences.

Compared with the weak interference, under the influence of strong interference, the noise fluctuation curve in the amplitude direction has a lower loss at zero detuning. At the far detuning, the noise curve changes from compression to amplification, and a three-peak structure appears. Similarly, in the phase direction, the strong interference changes from amplification to compression at the far detuning, while the weak interference remains in the amplification state. In addition, three depressions also appear. Therefore, it can be seen that the quantum manipulation under strong interference condition is more significant than that under weak interference condition, and appropriate changes in the phase of signal beam and pump beam will also have an appropriate impact on the quantum manipulation.

The nonlinear process of injection in a coupled vacuum compression cavity is theoretically studied. By adjusting the reflection coefficient of the intermediate cavity mirror, the quantum fluctuations under different interference conditions in the cavity can be observed. We found that the system has a higher degree of compression

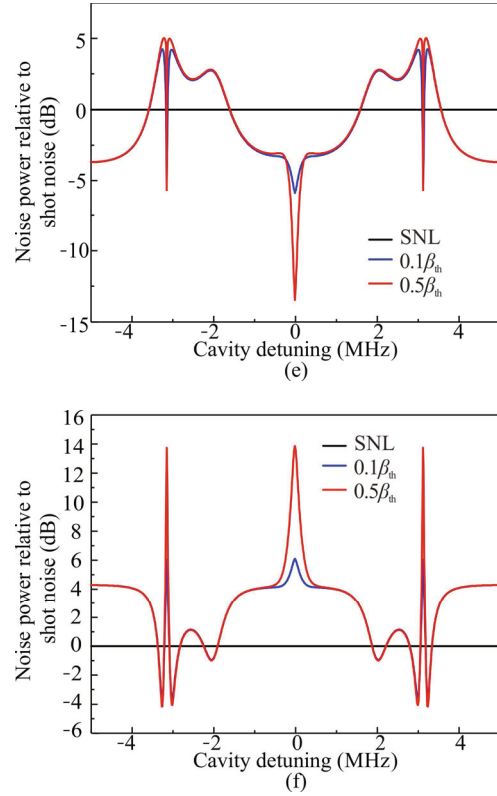
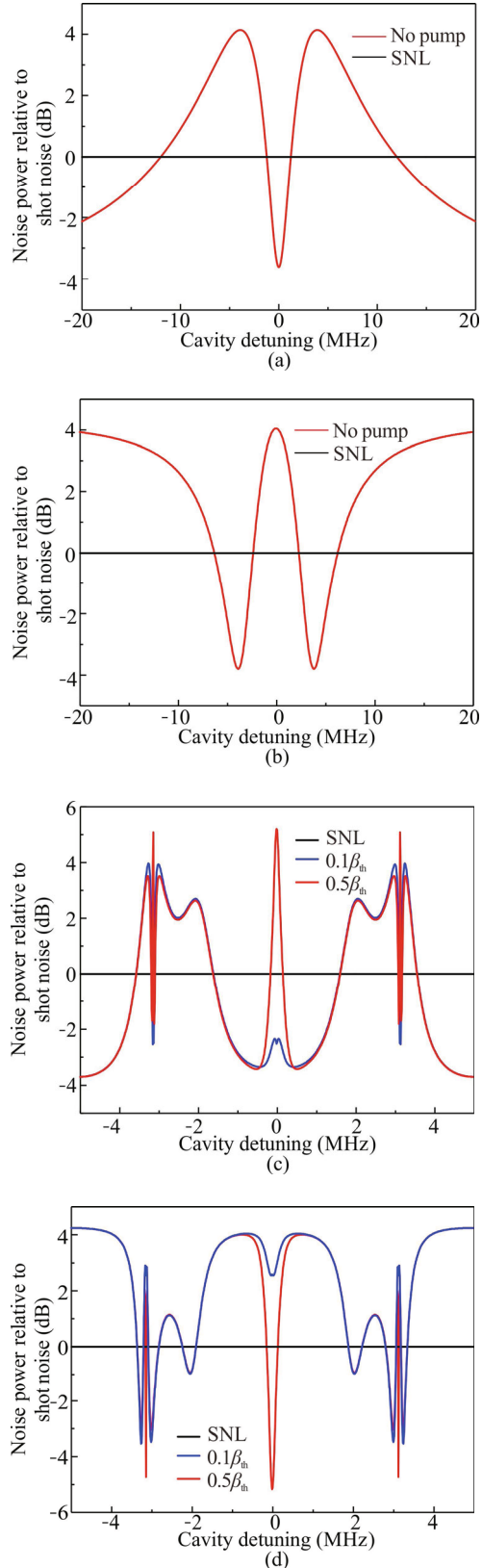


Fig.5 Quantum correlation noise fluctuation curves in the vacuum compression field of the strongly coupled resonant cavity under three resonance cases: Noise curves in the (a) amplitude and (b) phase directions without pump light injection; Noise curves in the (c) amplitude and (d) phase directions when $\theta=0$; Noise curves in the (e) amplitude and (f) phase directions when $\theta=\pi$

in the case of strong interference of the intermediate cavity mirror. At the same time, proper adjustment of the phase difference of the pump beam and signal beam will also enhance the effect of quantum manipulation. This work can be widely used in frontier fields, such as quantum key distribution, quantum state teleportation, and so on.

Statements and Declarations

The authors declare that there are no conflicts of interest related to this article.

References

- [1] WILK T, GAËTAN A, EVELLIN C, et al. Entanglement of two individual neutral atoms using Rydberg blockade[J]. Physical review letters, 2010, 104(1): 010502.
- [2] BROWAEYS A, BARREDO D, LAHAYE T. Experimental investigations of dipole-dipole interactions between a few Rydberg atoms[J]. Journal of physics B atomic molecular physics, 2016, 49(15): 152001.

- [3] LIN Y C, NABEKAWA Y, MIDORIKAWA K. Optical parametric amplification of sub-cycle shortwave infrared pulses[J]. Nature communications, 2020, 11(1): 3413.
- [4] TAYEBEH N, ZEYNAB M, MASOUMEH H M. White light cavity via electromagnetically induced transparency based four-wave mixing in four-level Rb atoms[J]. Applied physics A, 2020, 126(9): 674.
- [5] KUMAR S C, WEI J, DEBRAY J, et al. High-power, widely tunable, room-temperature picosecond optical parametric oscillator based on cylindrical 5% MgO:PPLN[J]. Optics letters, 2015, 40(16): 3897-3900.
- [6] WAGNER F, JOAO C P, FILS J, et al. Temporal contrast control at the PHELIX petawatt laser facility by means of tunable sub-picosecond optical parametric amplification[J]. Applied physics B, 2014, 116(2): 429-435.
- [7] ZHANG C, CHENG S, LI L, et al. Experimental validation of quantum steering ellipsoids and tests of volume monogamy relations[J]. Physical review letters, 2019, 122(7): 070402.1-070402.6.
- [8] HU J Y, HE J Y, LIU Y G, et al. Nonlinear propagation of pulses in multimode fiber with strong linear coupling[J]. Optoelectronics letters, 2020, 16(5): 379-383.
- [9] AOKI T, TAKAHASHI G, FURUSAWA A. Squeezing at 946nm with periodically poled KTiOPO₄[J]. Optics express, 2006, 14(15): 6930.
- [10] YU L, FAN J, ZHU S, et al. Creating a tunable spin squeezing via a time-dependent collective atom-photon coupling[J]. Physical review A, 2013, 89(2): 530-541.
- [11] YANG W, JIN X, YU X, et al. Dependence of measured audio-band squeezing level on local oscillator intensity noise[J]. Optics express, 2017, 25(20): 24262.
- [12] FULVIO F, FLAMINI F, WALSCHAERS M, et al. Validating multi-photon quantum interference with finite data[J]. Quantum science and technology, 2020, 5(4): 045005.
- [13] VAHLBRUCH H, MEHMET M, DANZMANN K, et al. Detection of 15dB squeezed states of light and their application for the absolute calibration of photoelectric quantum efficiency[J]. Physical review letters, 2016, 117(11): 110801.
- [14] ROMAN S. Squeezed states of light and their applications in laser interferometers[EB/OL]. (2017-12-17) [2021-09-01]. <https://arxiv.org/pdf/1611.03986.pdf>.
- [15] WAN Z, FENG J, LI Y, et al. Comparison of phase quadrature squeezed states generated from degenerate optical parametric amplifiers using PPKTP and PPLN[J]. Optics express, 2018, 26(5): 5531.
- [16] RAUSSENDORF R, BRIEGEL H J. A one-way quantum computer[J]. Physical review letters, 2001, 86(22): 5188-5191.
- [17] TAKAHIRO S, JUN-ICHI Y, KENZO M, et al. Creation and measurement of broadband squeezed vacuum from a ring optical parametric oscillator[J]. Optics express, 2016, 24(25): 28383-28391.
- [18] LI Z, SUN X, WANG Y, et al. Investigation of residual amplitude modulation in squeezed state generation system[J]. Optics express, 2018, 26(15): 18957-18968.
- [19] YANG W, SHI S, WANG Y, et al. Detection of stably bright squeezed light with the quantum noise reduction of 126 dB by mutually compensating the phase fluctuations[J]. Optics letters, 2017, 42(21): 4553.
- [20] WEI C H, ZUO C L, LIANG L, et al. Compact external cavity diode laser for quantum experiments[J]. Optoelectronics letters, 2020, 16(6): 433-436.
- [21] BRAVERMAN B, KAWASAKI A, VULETIĆ V. Impact of non-unitary spin squeezing on atomic clock performance[J]. New journal of physics, 2018, 20(10): 103019.
- [22] WANG L, TAN Z, ZHU Y, et al. Control of optical bistability in the nonlinear regime of two-sided cavity quantum electrodynamics[J]. Journal of the optical society of America B optical physics, 2017, 34(9): 1780.